



Impedance spectroscopy and membrane potential analysis of microfiltration membranes. The influence of surface fractality

Darío Ramón Díaz^a, Francisco Javier Carmona^b, Laura Palacio^c, Nelio Ariel Ochoa^a, Antonio Hernández^c, Pedro Prádanos^{c,*}

^a Laboratorio de Membranas y Biomateriales, Instituto de Física Aplicada, Universidad Nacional de San Luis-CONICET, Chacabuco 917, D5700BWS San Luis, Argentina

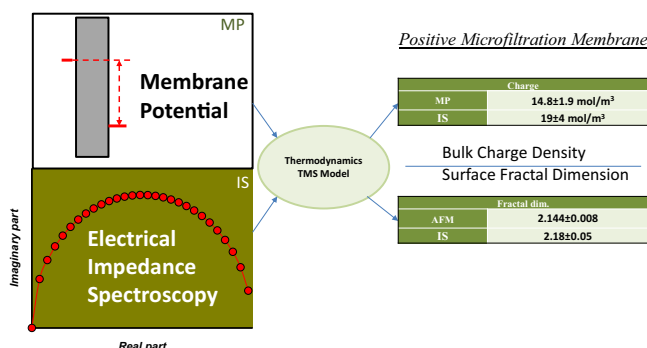
^b Dpto. de Física Aplicada, Escuela Politécnica, Universidad de Extremadura, 10004 Cáceres, Spain

^c Grupo de Superficies y Materiales Porosos, Dpto. Física Aplicada, Facultad de Ciencias, Universidad de Valladolid, 47071 Valladolid, Spain

HIGHLIGHTS

- The transport properties of a charged microfiltration membrane were studied.
- Membrane potential (MP) allowed a calculation of the transport numbers.
- Impedance Spectroscopy (IS) allowed to get electric conductivity inside the pores.
- Similar electrical proper charge was obtained from MP and IS methods.
- The roughness fractal dimension of the membrane surface was correlated with IS results.

GRAPHICAL ABSTRACT



ARTICLE INFO

Article history:

Received 14 July 2017

Received in revised form 29 November 2017

Accepted 14 December 2017

Available online 15 December 2017

Keywords:

Membrane surface charge density
Electrical impedance spectroscopy
Membrane roughness fractal dimension
Membrane potential
Transport numbers

ABSTRACT

In this work, the proper charge density of a microfiltration membrane has been determined by using two different methods. Firstly, the ionic transport of a KCl solution has been investigated by simultaneous measurements of saline flux and membrane potential (MP) resulting from a concentration gradient through the membrane. A simple model, including all the relevant contributions to the global electrical potential drop, allowed a calculation of transport numbers and membrane charge density.

The response of ions inside the membrane to an oscillating electrical potential has been analyzed by impedance spectroscopy (or electrical impedance spectroscopy EIS). A quite simple experimental EIS design allowed, by taking into account MP measurements too, an easy assignment of an equivalent circuit. After a careful analysis of EIS results, it was possible to evaluate the electrical conductivity inside the pores and the charge density. Both were found to be quite similar to the values obtained from MP alone. This agreement of EIS results with the MP ones, that are much simpler to deal with, confirms the accuracy of EIS to study the electrical properties of microfiltration membranes.

The influence of electrode roughness and, in our EIS cell, the membrane roughness, on the constant phase element (CPE) of the equivalent circuit has been proved. Within this frame, the roughness fractal dimension of the membrane surface could be determined from EIS measurements. It resulted in fair agreement with the atomic force microscopy (AFM) determination.

© 2017 Elsevier Ltd. All rights reserved.

* Corresponding author.

E-mail address: pradanos@termo.uva.es (P. Prádanos).

Nomenclature

Symbol list

A	membrane area exposed to flux
$(a_j)'$	activity at the corresponding interface offside the membrane of the j th species
$(\bar{a}_j)'$	activity at the corresponding interface inside the membrane of the j th species
(a_{\pm})	average activity of the electrolyte
$(a_{\pm})'$	average activity of the electrolyte at the corresponding interface offside the membrane
$(\bar{a}_{-})'$	activity at the corresponding interface inside the membrane of anion.
C_{pore}	Capacitance of the solution inside the pores
C	salt concentration
C'	salt concentration at the corresponding interface offside the membrane
c_j	concentration of ion j outside the membrane
\bar{c}_j	concentration of ion j inside the membrane
D_d	diffusivities through the diffusion layers
\bar{D}_m	membrane diffusion coefficient
D_f	fractal dimension
d_p	pore diameter
E_{cell}	cell potential
E_m	electric potential drop
E'_m	proper membrane potential
\bar{E}_{diff}	diffusion potential inside the pores
E_{lj}	liquid junction potential
E_{Nernst}	Nernstian contribution potential.
F	Faraday constant
G_{pore}	conductance inside the pores
I, I', II', II	successive interfaces encountered along the membrane system
j	saline flux; Imaginary number $\sqrt{-1}$
j_0	initial flux
K	constant in Eq. (25)
L	channel length
n	exponent relating impedance of CPE (Eqs. (22) and (23))
n'	slope of the function $\gamma(\sigma)$ in a double logarithmic scale
P_{ms}	permeability
Q	constant (measured in $F \cdot s^{n-1}$) of Eq. (23)
R	universal constant of gases
R_{pore}	resistance of the solution inside the pores
$r_{j,Stokes}$	Stokes radius of the j th species
r_{pore}	pore radius
T	temperature
t	time
t_j	transport numbers outside the membrane of the j th species
\bar{t}_j	transport numbers inside the membrane of the j th species
U	mobility outside the membrane
\bar{U}	mobility inside the membrane

V	volume of high and low concentration compartments (assumed equal to each other)
v	average tangential speed.
x	coordinate
X_m	proper membrane charge
Z	impedance
Z'	real component of the system impedance
Z''	imaginary component of the system impedance
z_j	ion valence of the j th species

Greeks letters

α	fraction of the pore section defined in Eq. (18)
δ	diffusion layer thicknesses
$\Delta W'_{j,Born}$	free energy difference due to Born effects
$\Delta W'_{j,im}$	free energy difference due to image
Δx	membrane thickness
$\Delta \Psi'$	Donnan's potential at the corresponding interface
$\Delta \Psi$	normalized Donnan's potential
ε	permittivity
ε_0	vacuum permittivity
ϕ_j	steric factor of the ion j
γ_j	activity coefficient of de ion j outside the membrane
$\bar{\gamma}_j$	ionic activity coefficient inside the membrane
γ_{\pm}	average activity coefficient of the electrolyte
$\gamma(\vec{\sigma})$	power spectra density function
η	viscosity of the solution
κ	conductivity
κ_{total}	total conductivity
μ_j	chemical potential of the j th species
$(\mu_j)'$	chemical potential at the corresponding interface outside the membrane of the j th species
$(\bar{\mu}_j)'$	chemical potential at the corresponding interface inside the membrane of the j th species
θ	membrane porosity
ρ	density of solution.
ω	angular frequency
ξ	sign (+1 or -1) of the membrane charge

Sub indexes

bulk	outside the membrane
high	high concentrations side in MP measurements
j	numeral/counter of species
low	low concentrations side in MP measurements
m	membrane
pore	pore
surface	surface
\pm	average
+	cation
-	anion

1. Introduction

The charge of a membrane controls its separation properties especially when dealing with electrolytes or any other charged species (Pinelo et al., 2013; Schaep et al., 1998; Tanninen et al., 2007). This is particularly true for ion exchange membranes. The charge, or its volume or surface density, and its sign play a key role in electrodialysis, with only secondary role for pore sizes, and its selectivity (Mikhaylin and Bazinet, 2016). In many other situations, the charge of the membrane, but also its dielectric properties, play

a significant enough role as to justify a careful investigation of these properties. This would help to predict the adequacy of a membrane for the desired application requirements (Xu, 2005).

Many experimental methods can be used to study the transport properties with proper charge or showing a certain charge when immersed in a charged solution, due for example to adsorption. Among others, we can mention: ionic permeability, streaming potential, streaming current, membrane potential, impedance spectroscopy, etc. (Benavente and Fernandez-Pineda, 1985; Hernandez et al., 1995; Lakshminarayanaiah, 1965; Martínez et al., 2002).

Here we will use both, membrane potential (MP) and electrical impedance spectroscopy (EIS). Although, MP is not always well applied or understood, it is a rather old and simple method (Nagasawa and Kobatake, 1952). It actually has a great potential because it can be dealt from several points of view including: Electrochemistry, Kinetics and Thermodynamics (Lakshminarayanaiah, 1984). Irreversible Thermodynamics is the theoretical frame most usually applied to treat charged membranes (Lakshminarayanaiah, 1975; Siddiqi et al., 1978) as well as to study other non-equilibrium complex systems.

We will focus on EIS which is a much less known technique, but we will use MP as an auxiliary tool and as a reference for comparison. The idea is to use these two concomitant methods to test the EIS technique when there is a relatively easy methodology to be compared to each other.

Impedance spectroscopy is a technique with a wide range of possibilities to characterize electric and dielectric properties of relevance to understand the transport through a membrane (de Lara and Benavente, 2007; Freger and Bason, 2007; Silva et al., 2016). This technique when applied to porous membranes has certain limitations that it is worth considering. Firstly, it is an invasive methodology because it requires placing electrodes in the membrane holder perturbing, to some extent, the membrane behavior (Chilcott et al., 2002). Moreover, it requires a pore model that should be as simple as possible without oversimplifications. Normally, the pores are taken as a bunch of parallel cylinders, although not always this is accurate enough (de Lara and Benavente, 2007). Finally, when dealing with multilayer membranes, they can cause overlapping of the semicircular plots on the Nyquist diagram (Silva et al., 2016).

The main advantages of EIS are its experimental simplicity and speed (EIS is a fast test with simple experimental requirements) (Cañas et al., 2001). One of its drawbacks is the uncertainty about the assignment of an equivalent circuit and the attribution of physically significant properties of the phenomena to study (Barsoukov and Macdonald, 2005; Bason et al., 2007; Freger and Bason, 2007; Romero et al., 2013). This is the reason why the system or process to be studied must be as simple as possible in order to avoid any undesired or not fundamental contribution to the global impedance. Besides, the technique requires a careful elimination of undesired signal sources as wiring and connections (Montalvillo et al., 2014; Zhao and Ni, 2011). Some ways to simplify the system under investigation by EIS are, for example: the elimination of the support layer of a composite membrane or the use of an experimental setup that could avoid the formation of diffusion layers at both sides of the membrane (Bason et al., 2007; Efligenir et al., 2015). This requirement of simplicity suggests the elimination of processes with relaxation times of the same, or similar, order of magnitude as those of the ions inside the pores of the membrane. The presence of many similar relaxation times obscures the Nyquist plot and gives a flattening of the imaginary versus real impedance arcs. This would require a not always easy, deconvolution process. In general, these distributions of relaxation times are quite inconvenient when the membrane has pore sizes over the nanometer range (Ariza et al., 2001; Zhao et al., 1991). There are also studies that correlate the presence of wide pore size distributions and roughness of the electrode surface with a widening of the relaxation time distribution. It is also generally known that roughness is a fractal magnitude, with self-similarity measured at different scales, thus allowing evaluating the surface fractal dimension (Macdonald, 1987). Given that roughness and fractality can be independently evaluated by atomic force microscopy (AFM), we will explore this correlation here.

In this work we will show how to get the membrane charge of a microfiltration membrane and its ion transport properties with the two complimentary techniques of MP and EIS. Moreover, we will

explore the possible to evaluate a structural characteristic of the membrane surfaces, as their fractal dimension, by an electrical analysis tool as EIS. Our general goal is to test and validate the accuracy of EIS to give an insight of the mechanisms acting on and inside a microfiltration membrane.

2. Theory

2.1. Ionic permeability

Saline diffusion driven by a concentration gradient through a membrane can be considered as stationary after a short (few seconds) time lag. Then, the saline flux, j , is:

$$j = P_{ms}(C_{high} - C_{low}) \quad (1)$$

where C_{high} and C_{low} are the salt concentrations at both sides of the membrane system and P_{ms} is the permeability (see Fig. 1). Considering that:

$$j = \frac{V}{A} \frac{dC_{low}(t)}{dt} = -\frac{V}{A} \frac{dC_{high}(t)}{dt} \quad (2)$$

with V the volume of high and low concentration compartments (assumed equal to each other) and A being the membrane area exposed to flux. It can be shown (Lonsdale et al., 1965; Martínez-Villa et al., 1988) that:

$$C_{low} = C_{low}(0) + [C_{low}(\infty) - C_{low}(0)] \left[1 - \exp\left(-\frac{2AP_{ms}t}{V}\right) \right] \quad (3)$$

If linear concentration gradients are assumed through the proper membrane (with thickness Δx) and through the adjoining diffusion layers (with thicknesses δ_{high} and δ_{low}):

$$j = D_d \frac{(C_{high} - C'_{high})}{\delta_{high}} = \bar{D}_m \frac{(\bar{C}_{high} - \bar{C}_{low})}{\Delta x} = D_d \frac{(C'_{low} - C_{low})}{\delta_{low}} \quad (4)$$

Here, the diffusivities through the diffusion layers, D_d , have been assumed as equal for both the layers and the bulk solution but different from that through the membrane. The membrane diffusion coefficient will be \bar{D}_m (see again Fig. 1).

2.2. Membrane potential

The difference in the ionic mobilities caused by the presence of a membrane leads to an electrical potential through it. When the membrane is charged, the Donnan equilibrium have to be taken into account in such a way that the electrical potential drop along all the layers and interfaces appearing in the system is (Lakshminarayanaiah, 1965, 1969):

$$E_m = \frac{1}{F} \int_I^{I'} \sum_{j=1}^n \frac{t_j}{z_j} \cdot \nabla \mu_j dx + (\Delta \Psi'_{high}) + \frac{1}{F} \int_{I'}^{II'} \sum_{j=1}^n \frac{\bar{t}_j}{z_j} \cdot \nabla \mu_j dx + (\Delta \Psi'_{low}) + \frac{1}{F} \int_{II'}^{II} \sum_{j=1}^n \frac{t_j}{z_j} \cdot \nabla \mu_j dx \quad (5)$$

with I, I', II' and II referring to the successive interfaces encountered along the membrane system. F is the Faraday's constant, z_j is the elemental charge of the j th species, μ_j is its chemical potential, t_j its transport number outside the membrane while \bar{t}_j refers to the membrane itself. In Fig. 1, \bar{E}_{diff} refers to the third term of Eq. (5) and stands for the diffusion potential inside the pores. The Donnan's potentials are:

$$\Delta \Psi'_{high} = \frac{RT}{z_j F} \ln \frac{(a_j)'_{high}}{(\bar{a}_j)'_{high}} = \frac{1}{z_j F} [(\mu_j)'_{high} - (\bar{\mu}_j)'_{high}] \quad (6)$$

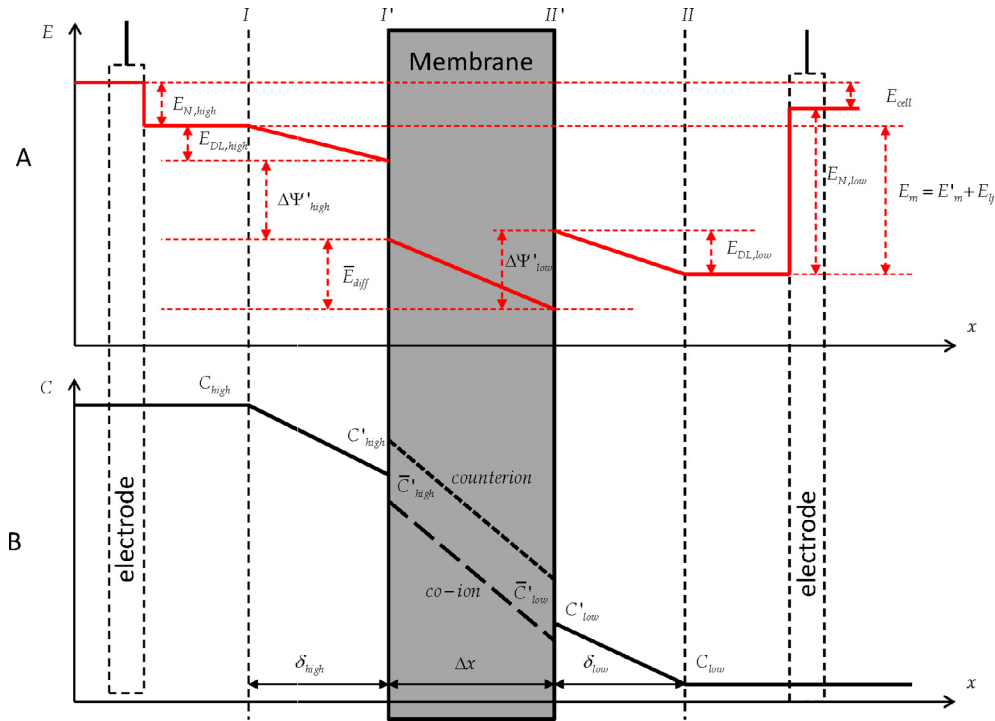


Fig. 1. Scheme of the different layers and interfaces through the membrane system. A: Potential profile assuming electrodes selective to the counterion. B: Concentration profiles.

and a similar expression for $\Delta\Psi'_{low}$. Here $(a_j)'_{high}$ is the activity at the corresponding interface outside the membrane and $(\bar{a}_j)'_{high}$ corresponds to the membrane inside of the interface.

If a simple salt (1:1) solution is assumed:

$$E_m = \frac{RT}{F} \left[\Delta t \ln \frac{(a_{\pm})'_{high}}{(a_{\pm})'_{low}} + (\Delta \bar{t} - \Delta t) \ln \frac{(a_{\pm})'_{high}}{(a_{\pm})'_{low}} - \left(1 - \sum \bar{t}\right) \ln \frac{(\bar{a}_{-})'_{high}(a_{\pm})'_{low}}{(\bar{a}_{-})'_{low}(a_{\pm})'_{high}} \right] \quad (7)$$

(a_{\pm}) being the average activity of the electrolyte. Moreover:

$$\begin{aligned} \Delta t &= t_- - t_+ \\ \Delta \bar{t} &= \bar{t}_- - \bar{t}_+ \\ \sum \bar{t} &= \bar{t}_- + \bar{t}_+ \end{aligned} \quad (8)$$

In Eq. (7) the first term stands for the liquid junction potential, E_{ij} . Then the proper membrane potential is:

$$E'_m = \frac{RT}{F} \left[(\Delta \bar{t} - \Delta t) \ln \frac{(a_{\pm})'_{high}}{(a_{\pm})'_{low}} - \left(1 - \sum \bar{t}\right) \ln \frac{(\bar{a}_{-})'_{high}(a_{\pm})'_{low}}{(\bar{a}_{-})'_{low}(a_{\pm})'_{high}} \right] \quad (9)$$

Of course, $\sum \bar{t} \neq 1$ because part of the total current would be transported as a surface current on the pore walls inside the membrane.

For a membrane having a charge X_m , E'_m would be:

$$E'_m = \frac{RT}{F} \left[(\Delta \bar{t} - \Delta t) \ln \frac{(a_{\pm})'_{high}}{(a_{\pm})'_{low}} + \left(\frac{X_m}{2(a_{\pm})'_{high}} \left(\frac{(a_{\pm})'_{high}}{(a_{\pm})'_{low}} - 1 \right) \right) (1 - \sum \bar{t}) \right] \quad (10)$$

Once electroneutrality has been taken into account, Eq. (10) allows the determination of transport numbers inside the pores and membrane charge from proper membrane potentials. This would require knowing activities on the membrane at the high and low interfaces. Fortunately these activities can be evaluated according to Eq. (4), if the thickness of the diffusion layers is known, from measurements of saline flux.

2.3. Dielectric analysis

The impedance spectroscopy technique is based on measurements of electrical impedance as a function of frequency. An equivalent circuit can be proposed to each system analyzed that could adapt to the characteristics of the response obtained. An ulterior analysis of the physical processes that would correspond to the characteristics of the equivalent circuit would give relevant information on the system studied.

The non-linearity of signal-response relationship can be a serious problem that in turn can be easily minimized by keeping the signal low but, over the thermal noise level (Macdonald, 1987). Of course, it is still possible that the process itself were as complex as to include wide relaxation time distributions that would introduce intrinsic non-linearity. In order to simplify the equivalent circuit needed, the experimental device should be as simple as possible.

In our case, we use mercury (Hg) in contact with the membrane at both sides of it, what constitutes electrodes approximately perfectly polarizable. These electrodes can be represented by a condenser in parallel with a high resistance (infinite for a perfect polarizable electrode) (Starzak, 1984). In this way, the system can be outlined as shown in Fig. 2a. The equivalent circuit consists in two elements in series, corresponding to the solution inside the pores and to the electrode-solution interface, respectively. This model is shown in Fig. 2b and the corresponding ideal Nyquist plot is shown in Fig. 2c. The relaxation constants will be different enough as to allow two independent lobes to appear in the corresponding Nyquist plot. The lower frequency lobe varies with the electric potential applied, which usually corresponds to a polarization layer normal to the electric field (Montalvillo et al., 2014).

The first lobe allows a determination of resistance and capacitance of the solution inside the pores, R_{pore} and C_{pore} . This requires an elimination of the effect of the polymeric matrix of the membrane by the appropriate experimental procedure (Open/Short/Load measurements) detailed in Section 3.4 below. When all pores

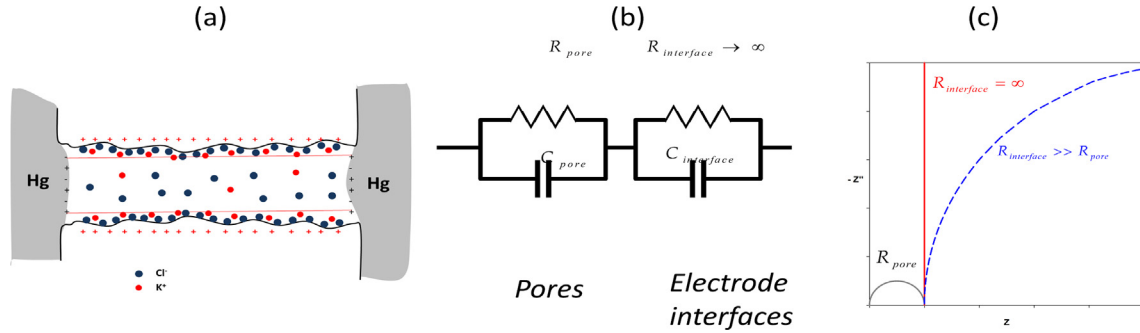


Fig. 2. (a) Scheme of the situation during IS measurements in a membrane pore containing a KCl solution. (b) Equivalent circuit, (c) Nyquist plot for the equivalent circuit.

can be assumed to be identical cylinders perpendicular to the membrane surfaces, the first lobe should be a perfect semi-circle with a single relaxation time (Debye response) (Macdonald, 1987). Actually, there are pores differently inclined and with different shapes. This leads to pore size and length distributions giving a distribution of relaxation times that cause a flattening of the semi-circle in the Nyquist plot. Some authors correlate these flattened lobes to the surface fractality that would appear due to the roughness and size distribution of open pores (Pajkossy, 1991).

2.4. Relative permittivity and conductivity inside the pores

The conductance inside the pores, if parallel pores are assumed, is the sum of the conductance inside all the n pores:

$$G_{pore} = \frac{1}{R_{pore}} = \sum_{i=1}^n \frac{1}{R_i} = \sum_{i=1}^n G_i \quad (11)$$

Conductivity is:

$$\kappa_{pore} = G_{pore} \frac{\Delta x}{A \theta} \quad (12)$$

Here θ is the membrane porosity. In the same way, the capacitance inside the pores is:

$$C_{pore} = \sum_{i=1}^n C_i \quad (13)$$

and the permittivity:

$$\epsilon_{pore} = C_{pore} \frac{\Delta x}{A \theta \epsilon_0} \quad (14)$$

with ϵ_0 the vacuum permittivity.

2.5. Thermodynamic equilibriums at the interfaces

Two thermodynamic equilibriums are established at the interfaces because of the presence of ions outside and inside the membrane (Bowen and Welfoot, 2002; Yaroshchuk, 2001). These equilibriums require the following relationship to hold at both membrane-solution interfaces:

$$\frac{c_j}{\bar{c}_j} = \phi_j \frac{\bar{\gamma}_j}{\gamma_j} \exp(-z_j \Delta \Psi) \exp(-\Delta W'_{j,Born}) \exp(-\Delta W'_{j,im}) \quad (15)$$

Here \bar{c}_j stands for the concentration inside the membrane and c_j for the concentration outside the membrane; $\bar{\gamma}_j$ and γ_j are the corresponding activity coefficients; ϕ_j takes into account the steric effect; $\Delta \Psi$ is the normalized Donnan potential. Dielectric effects consist in the Born contribution, $\Delta W'_{j,Born}$, and those of image forces $\Delta W'_{j,im}$ (Montalvillo et al., 2014; Silva et al., 2016). When dealing with wide enough pores (as is the case of microfiltration mem-

branes), the Stokes radii of the ions is much less than the pore radii $r_{j,Stokes} \ll r_{pore}$ and consequently $\phi_j \rightarrow 1$ and $\epsilon_{pore} = \epsilon_{bulk}$. But when the permittivities inside and outside the pore are equal, the Born contribution to the equilibrium is zero. Moreover, both the Bjerrum radii (the distance between the ions above which their electrostatic interaction is lower or comparable to thermal energy) and the Debye length are much smaller than the pore radii. This would lead to null image contributions in the equilibrium (Silva et al., 2016). The dielectric constant could be affected into highly charged membranes what would make necessary a consideration of the dielectric effects and have a certain influence on the Donnan equilibrium itself (Cwirko and Carbonell, 1992). Nevertheless, because our membranes have moderate to low proper charges we are not going to consider these possibilities.

If Donnan equilibrium is still considered, Eq. (15) becomes:

$$\frac{a_j}{\bar{a}_j} = \exp(-z_j \Delta \Psi) \quad (16)$$

Attending to the simple procedure to deal with the Donnan contribution it is convenient to retain it even with microfiltration membranes (Kontturi et al., 1994; Takagi and Nakagaki, 1996). Moreover, note that otherwise $a_j \simeq \bar{a}_j$ what seems a too strong assumption to start with.

The equilibrium conditions can be taken into account to compare the inside and outside conductivities by Lakshminarayanaiah (1965):

$$\begin{aligned} \frac{\kappa_{pore}}{\kappa_{bulk}} &= \frac{\bar{U}_+ \bar{t}_+}{U_+ t_+} \left(\sum \bar{t} \sqrt{\left(\frac{X_m}{2a_{\pm}} \right)^2 + 1} + \xi(\Delta \bar{t}) \frac{X_m}{2a_{\pm}} \right) \\ &= \frac{\bar{U}_- \bar{t}_-}{U_- t_-} \left(\sum \bar{t} \sqrt{\left(\frac{X_m}{2a_{\pm}} \right)^2 + 1} + \xi(\Delta \bar{t}) \frac{X_m}{2a_{\pm}} \right) \end{aligned} \quad (17)$$

The parameters \bar{U}_+ , U_+ , \bar{U}_- and U_- are the cation and anion mobilities, inside (barred) and outside (unbarred) the membrane, for both, the cation and anion, and ξ takes into account the sign (+1 or -1) of the membrane charge.

Eq. (17) is based on the TMS (Teorell-Meyer-Sievers) model (Tanaka, 2015). The adequacy of the TMS model has been discussed mostly when compared to the space charge model (SC) whose validity was tested by Westerman-Clark and co-workers (Christoforou et al., 1985; Westermann-Clark and Anderson, 1983). Palmeri and co-workers have investigated this question for nanofiltration membranes (Palmeri et al., 1999, 2000). Some light was shed on this issue by Shang et al. (2006) by using simulations that showed that for pore radii over Debye's length ratios, r_p/λ_D with $\lambda_D = \sqrt{\frac{\epsilon RT}{2F^2 C_f}}$ for a 1:1 electrolyte, small (narrow pores and/or low concentrations) and big (wide pores and/or high concentrations) and for X_m/C_f high enough both the TMS and the SC

models lead to quite similar results. According to the recent considerations of Galama et al. (2016), in essence the range of validity of the TMS model embraces highly overlapping electrical double layers (low concentrations or high charges) or no overlapping double layers (high concentrations or low charges). Finally, as showed by Palmeri et al. (2000), the predictions of both the TSM and SC models differ from each other near to the conditions mentioned by far less than with experimental results. In our case, as will be seen in Section 4.3, we are in the high X_m/c_f and r_p/λ_D which guarantees that the TMS model can be used. These application ranges are wider for a 1:1 electrolyte than for an asymmetric one.

In systems like that outlined in Fig. 2a, with the presence of a surface charge density spread on the inner surface of a cylinder, a surface conductivity appears in such a way that the global conductivity can be represented by two parallel conduction circuits (Fievet et al., 2001; Lyklema and Minor, 1998; Yang et al., 2003). One of them would take place along the walls of a thin cylinder with a relatively high charge density uncompensated by the proper charge of the membrane on the pore surface. Some authors model this assuming that counter-ions would jump from site-to-site of fixed charge (Mafe et al., 2003). This could also be due to a high charge density due to the electrical double layer (Lakshminarayanaiah, 1984). This circuit would be in parallel with that along the center of the cylindrical pore where much less density of uncompensated charge would participate in current. Then the total conductivity would be (Lakshminarayanaiah, 1984):

$$\kappa_{\text{total}} = \alpha \kappa_{\text{surface}} + (1 - \alpha) \kappa_{\text{pore}} \quad (18)$$

α stands for the fraction of the pore section corresponding to the ring consisting in the transversal section of the high charge cylindrical layer on the pore surface. Clearly the thickness of the high charge shell must be of the order of the Debye's length, therefore it is $\alpha \ll 1$ for wide enough pores (and or low enough concentrations), and then:

$$\kappa_{\text{total}} = \alpha \kappa_{\text{surface}} + \kappa_{\text{pore}} \quad (19)$$

This is because $\kappa_{\text{pore}} < \kappa_{\text{surface}}$. It is worth noting that α obviously depends on concentration as expected due to its correlation with Debye's length.

Then Eq. (17) can be modified to read:

$$\frac{\kappa_{\text{total}}}{\kappa_{\text{bulk}}} = \frac{\bar{U} - t_-}{U - \bar{t}_-} \left(\sum \bar{t}_i \sqrt{\left(\frac{X_m}{2a_{\pm}} \right)^2 + 1} + \xi(\Delta \bar{t}) \frac{X_m}{2a_{\pm}} \right) - \frac{\alpha \kappa_{\text{surface}}}{\kappa_{\text{bulk}}} \quad (20)$$

3. Experimental

3.1. Membrane

We have used a microfiltration membrane shaped as disks of 47 mm in diameter and called SP02C. It is made of polyamide (Nylon 66) by Spectrum Laboratories (Rancho Dominguez, CA, USA). It has a nominal pore size of 0.2 μm , with a high chemical compatibility and can be used up to a maximal temperature of 130 $^{\circ}\text{C}$.

3.2. Structural characterization

A Nanoscope Multimode IIIa[®] scanning probe microscope from Digital Instruments (Veeco Metrology Inc., Santa Barbara, CA, USA) has been used to perform tapping mode Atomic Force Microscopy (AFM). Other details of the experimental AFM procedure follow the lines shown elsewhere (Silva et al., 2016).

The corresponding surface pore size distributions have been obtained by image analysis (Carvalho et al., 2011) with the ImageJ[®]

software (Abramoff et al., 2004). They have also been obtained with a Coulter Porometer II, which detects open pores because it uses a gas-liquid displacement method. The details of the experimental technique are given by us elsewhere (Hernández et al., 1996; Jacob et al., 1998). The volume porosity of the membrane has been evaluated by using a pycnometric method described elsewhere (Hernández et al., 1986).

Finally, the membrane thickness has been measured by using an electromagnetic induction device, the Dualscope^(C) MP03 from Fisher.

3.3. Saline permeability and electric potential

A membrane disk was placed between two matching methacrylate semi-cells of 8.55 cm^2 of active area. At both sides of the membrane, a flux of 0.6 L/min was set tangentially to reduce the concentration polarization effect. KCl solutions were used with a constant high concentration ($c_{\text{high}} = 2 \text{ mol/m}^3$) and low concentrations in the range $0.02 \text{ mol/m}^3 < c_{\text{low}} < 1 \text{ mol/m}^3$. Each membrane sample was conditioned during 24 h of immersion in a solution with the concentration c_{low} . Each semi-cell was fed from equal 0.56 L reservoirs. Two solution reservoirs feeding the semi-cells were leveled to maintain equal hydrostatic pressure at both sides of the membrane. A thermostatic bath kept a constant temperature of $298 \pm 1 \text{ K}$. Concentrations are measured in the compartment of low concentrations, $C_{\text{low}}(t)$, with a conductivity meter, while in the high concentration semi-cell, $C_{\text{high}}(t)$, is evaluated by the corresponding mass balance. These balances do not consider any water counter-transport (direct Osmosis) because any difference in the levels of both the reservoirs is detected.

Simultaneously with the saline flux, electric potential was measured with two Cl^- selective electrodes, ISE 9652 from Crison (Hach-Lange, Danaher Corporation, Washington, D.C., United States) placed at each side of the cell through a high impedance voltmeter. A description of this device can be seen in Silva et al. (2011).

Although the membrane is supposed to be symmetrical, AFM pictures show some differences from side to side of the membrane. Thus, the electric potential has been carried out with both sides facing the high concentration compartment. Quite similar values for the resulting potential have been obtained and the average has been used.

The cell potential, E_{cell} corresponds to the direct measurement by the voltmeter. The membrane potential E'_m includes the electric potential drop through the diffusion layers, the membrane and the corresponding interfaces. As shown in Fig. 1 ($E'_m = E_{\text{cell}} - E_{\text{Nernst}} - E_{ij}$) it is the cell potential minus the Nernstian potential and the liquid junction potential. The Nernstian contribution due to the concentration differences at both the electrode-solution interfaces, E_{Nernst} , has been previously measured as described by us elsewhere (Silva et al., 2016). E_{ij} is the liquid junction potential that for KCl is quite small, because both the ions have similar mobilities, nevertheless it has been accounted for. It is worth noting that E_{Nernst} is associated with the concentration jump at both electrode interfaces while E_{ij} refers to the concentrations in the bulk at both sides of the membrane.

3.4. Impedance spectroscopy

In order to perform impedance spectroscopy, a disk sample was placed between two nylon semi-cells, with a circular area of 10 mm diameter open to the flux, as shown in Fig. 3. It is a device similar to that used by Efligenir et al., to measure dielectric properties of a nanofiltration membrane (Efligenir et al., 2015). Both semi-cells are filled with the solution, which is displaced by mercury

that acts as an electrode directly contacting the membrane sample (and the solution filling the pores) at both of its sides. The measuring circuit is closed by using Pt electrodes dipped in the mercury. To isolate the system from any external electromagnetic field, the device is placed inside a stainless steel vessel that acts as a Faraday shield. In all cases, the membrane was conditioned for 24 h by immersing it into the salt solution prior to any experiment. Each concentration was measured 5 times with a high reproducibility. Deviations below 1% were observed for impedances at each frequency.

Impedance measurements were performed with a Solartron 1260 (Ametek, Berwyn, PA, United States) with frequencies from 10 MHz to 10 mHz and under 10 mV applied AC voltage. It has been tested that a 10 mV signal is over the thermal noise limit. The equipment is controlled by the Solartron Analytical software. EIS measurements were repeated for increasing concentrations going from 0.02 to 2 mol/m³. These solutions were made with Milli-Q deionized water, at 298 ± 1 K.

In order to eliminate the influence of wiring and any other electronic noise, an Open/Short/Load correction has been performed as described elsewhere (Montalvillo et al., 2014). Here the “short” measurement is done without the membrane in such a way that the mercury of both the semi-cells is in contact with each other. The “open” measurement is done by using a dry membrane in between both electrodes, what helps to eliminate the influence of the dry polymeric matrix. The “load” measurement is done with a 100 Ω resistance. The Open/Short/Load correction has to be taken into account to correct the outcomes for each frequency (Honda, 2009).

4. Results and discussion

4.1. Membrane parameters

The pore size distribution has been obtained by air-liquid porometry (Fig. 4a) and by AFM on both sides of the membrane (Fig. 4b). Note that, as can be seen in the insert of Fig. 4b, the differences in pore appearance on both sides are quite small and the pore size distribution shown has been obtained by averaging the results for both sides of the membrane. It is clear that the pore size distribution obtained by air-liquid porometry is more linked to the real opened pores and has therefore a more direct correlation with the membrane function. A comparison of both the distributions shows that air-liquid porometry (active pores) is much narrower than that for the surface openings. This would mean that most of the pores are narrower inside the membrane than on the surface. The distribution parameters obtained by fitting to a log-normal are shown in Table 1. There $\langle dp \rangle$ is the average pore size and σ is the standard deviation of the size distribution.

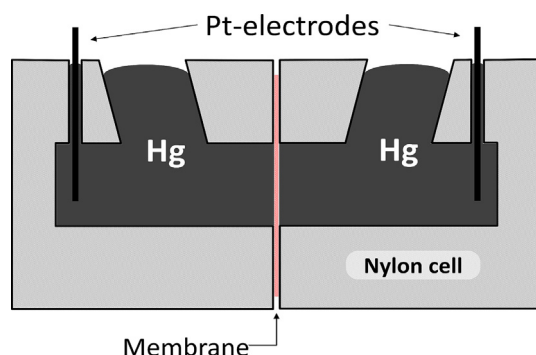


Fig. 3. Outline of the cell used in Impedance Spectroscopy.

The air-liquid porometry distribution is quite symmetrical and, when fitted to a Gaussian, gives $d_p = 0.34 \pm 0.04 \mu\text{m}$. The membrane thickness is $135 \pm 1 \mu\text{m}$, and the membrane volume porosity is $(69.9 \pm 0.5)\%$.

4.2. Ionic flux and membrane potential

The permeability can be obtained by a non-linear fitting of Eq. (3) to the concentration data in the low concentration compartment versus time. To make more evident the correlation of permeability and concentration, data have been presented as shown in Fig. 5 where Eq. (3) would correspond to straight lines. For the highest concentration in the range used for the low concentration compartment, a short initial time lag can be observed (see Fig. 5) while for lower concentrations a constant flux is obtained without a detectable time lag. This time lag can be correlated with the establishment of the electric double layer and the boundary layer which would be especially slow when water counter-transport appears. Although it could be affected by other experimental transitory effects, it should be determined by concentration gradients as far as it is hard to detect for low concentration gradients.

Straights shown in Fig. 5 correspond to fittings performed for times greater than 240 s. For all concentration gradients the correlation is over 0.9999. It can be seen a slight deviation from linearity for long times (over 1300 s) and the highest concentration in the low concentration compartment. This means that permeability is not constant for these long times. For the rest of concentrations, permeability is fully constant for both short and long times.

As can be seen in Fig. 6a, permeability decreases when concentration gradient increases. This should be correlated with the effect of direct osmosis because when the concentration gradient increases so does water counter-transport decreasing saline permeability.

Eq. (1) enables the evaluation of the flux through the membrane system. Saline flux changes with time as far as low concentration changes with time. The initial flux, j_0 , can be evaluated from the linearized fittings appearing in Fig. 5 and plotted against the difference of concentrations as shown in Fig. 6b. It appears clear, in this figure, that the initial flux is quite constant except for the highest low concentration used on the low concentration side of the membrane. It is worth noting that initial time lags (see Fig. 5) were eliminated and the flux registered after one additional minute was taken as j_0 . This additional minute were used because potential measurements had this duration.

According to Eq. (4), which is valid in stationary conditions, once δ_{high} and δ_{low} are known, we could obtain the concentration on the membrane at both its sides. The diffusivity in the diffusion layers, D_d , as mentioned, equals that of the bulk solution, that for the concentrations range can be taken as constant $D_d = (1.97 \pm 0.01) \cdot 10^{-9} \text{ m}^2/\text{s}$ (it would actually change in the third significant digit (Robinson and Stokes, 2002)).

The thickness of the diffusion layers can be investigated within the frame of dimensional analysis. Here we deal with a tangential solution flow of 0.6 L/min, this tangential flow leads to a Reynolds number of 658 (obtained by taking into account the channel dimensions in the measuring cell along with pure water values for density and viscosity and the value of D_d). This Re number falls within the laminar flow range. Moreover, the length of total development of the velocity layer is longer than the proper length of the channel. All these factors would advise to use the Grober's correlation in order to evaluate the diffusion layer thickness (Cheryan, 1986).

$$\delta = \frac{1}{0.664} \left(\frac{L^3 \eta D^2}{v^3 \rho} \right) \quad (21)$$

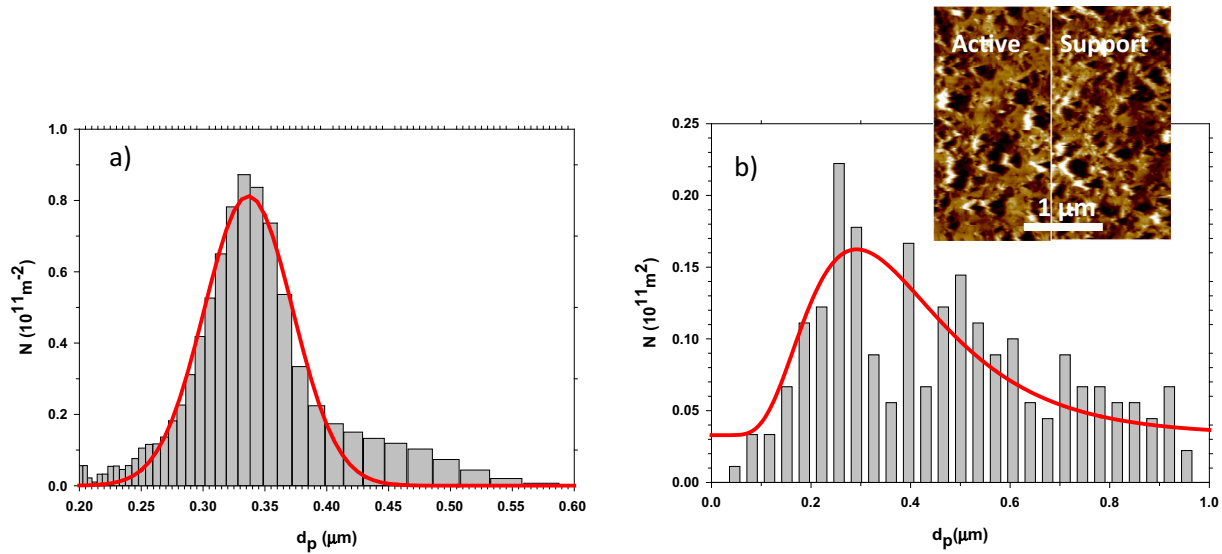


Fig. 4. Pore size distribution from (a) Air-liquid porometry, (b) Image analysis for AFM images.

Table 1
Parameters of the pore size distribution.

Technique	$\langle d_p \rangle$ (μm)	σ (μm)
AFM-images	0.36	0.46
Air-liquid porometry	0.34	0.10

Here, v is the average tangential speed, η is the shear viscosity, L is the channel thickness, and ρ is the mass density of the solution. Eq. (21) shows that the layer thickness depends on concentration mainly through diffusivity that in our concentration range is quite independent of concentration thus leading to $\delta_{\text{high}} = \delta_{\text{low}} = 43 \mu\text{m}$.

Then using Eq. (4), the concentrations on the membrane, C'_{low} and C'_{high} , can be evaluated as mentioned. The Debye–Hückel

theory (Robinson and Stokes, 2002) enables the calculation of activity coefficients, for diluted solutions up to 0.1 M of ionic strength.

In accordance with Eq. (10), E_m can be fitted as a function of activities, to get transport numbers inside the membrane along with the membrane charge. To do that, the transport numbers of the free solution have been taken as $t_+ = 0.4905$ and $t_- = 0.5095$. The fitted surface is shown in Fig. 7 and the corresponding values of transport number and charge for the membrane are shown in Table 2.

It can be seen in Table 2 that the K^+ transport number is reduced due to the positive membrane charge, this reduction is substantial although the membrane charge is moderate (Demisch and Pusch, 1979). These curve fittings, and those mentioned in

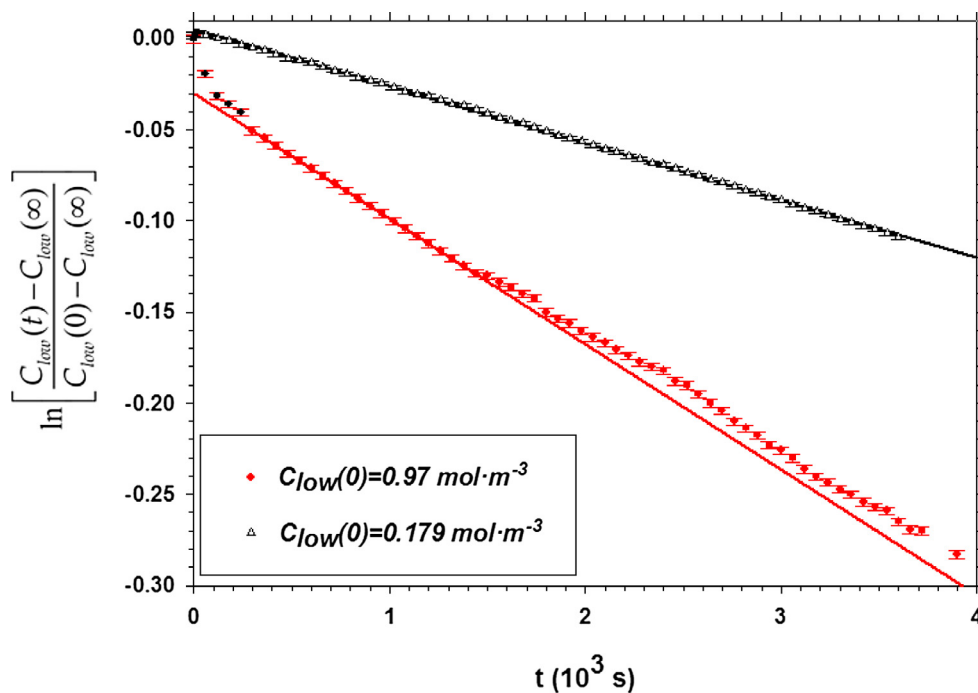


Fig. 5. Variation of C_{low} versus time.

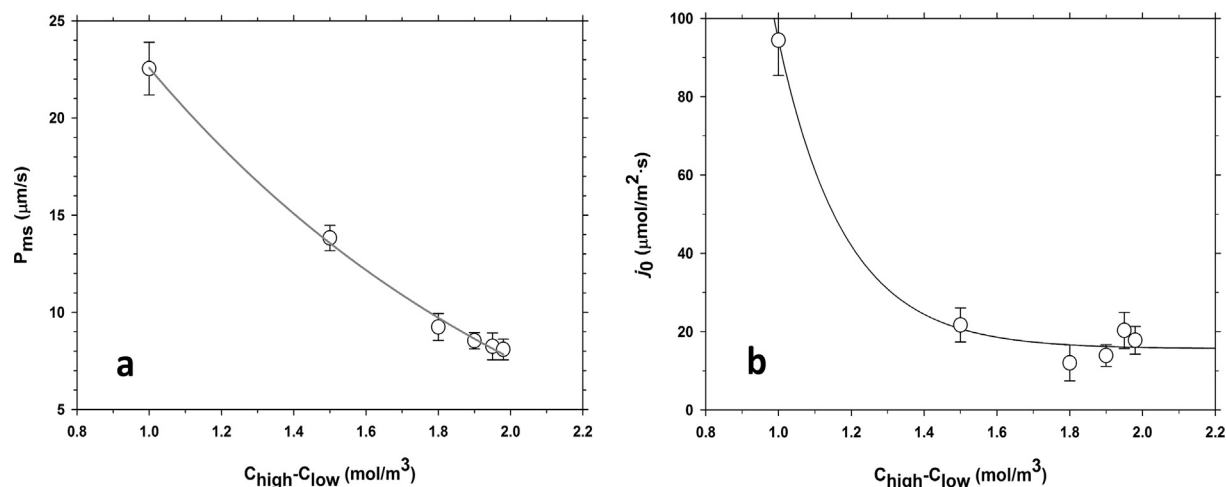


Fig. 6. Permeability (a) and initial saline flux (b) as a function of concentrations difference.

the following section, have been performed with SigmaPlot v11.0 (Systat Software Inc.), that uses the Marquardt-Levenberg algorithm, to find the coefficients (parameters) of the independent variable(s) that give the best fit between the equation and the data. Convergence did not depend, within wide physically meaning ranges, on the initial guess parameters.

4.3. Impedance spectroscopy

An example of the results obtained with IS for KCl solutions is shown in Fig. 8 using the Nyquist's plot. The first lobe, corresponds to high frequencies (low real impedances) and the beginning of a second lobe for lower frequencies (higher real impedances). The second lobe shows an important dependence of impedance with the average applied potential, which could be due to a diffuse double layer built by the ions in the solution on the mercury interface and its partially polarizable character.

The second lobe corresponds to a resistance much higher than that for the lobe of high frequencies. An infinite resistance would correspond to a perfectly polarizable electrode (Barsoukov and

Table 2

Membrane charge and transport numbers.

\bar{t}_+	0.12 ± 0.05
\bar{t}_-	0.82 ± 0.02
X_m	$14.8 \pm 1.9 \text{ mol/m}^3$

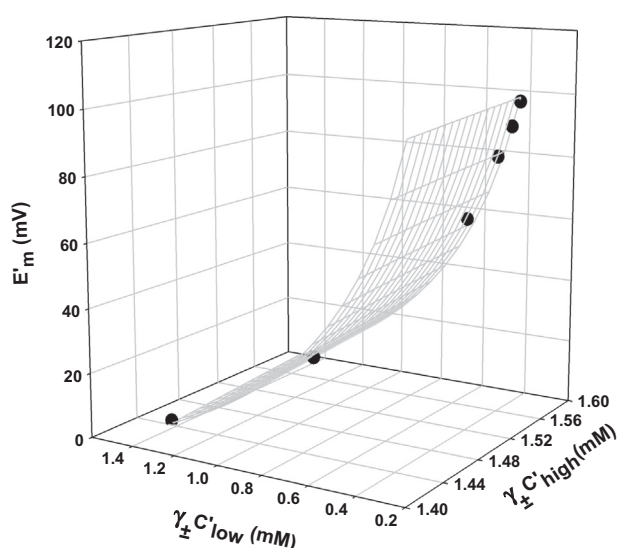


Fig. 7. Membrane system potential versus the product of the average activity coefficient and concentration of the solution in contact with the membrane. Grey-networked surface correspond to the best fit of Eq. (10).

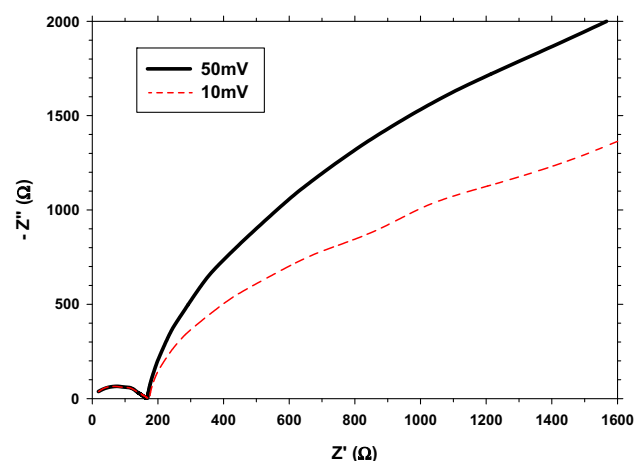


Fig. 8. Nyquist plot for KCl solution 2 mol/m^3 for applied potentials of 10 mV and 50 mV.

Macdonald, 2005). The first lobe is unaffected by the applied potential up to high potentials. Therefore, the corresponding equivalent circuit would give information on the dielectric and electric properties of the solution inside the membrane pores.

In Fig. 9a, the lobe of high frequencies in the Nyquist plot is shown for different concentrations. The size of this lobe increases as concentration decreases due to the less number of conducting ions inside the pores. This first lobe is not a perfect semi-circle but is actually quite close to it. Several possible circuits have been fitted (see Fig. 9b), with quite similar results. In order to decide what circuit to select, errors can be quantified by averaging the deviations from experimental data and their predictions for all the concentration range. This leads to the following relative errors: 2.80% for $R1||CPE1$, 2.95% for $R1||C1$ and 3.10% for $R1||C1 - R2$. It seems therefore that a better quality of fitting is obtained for the circuit including a constant phase element (CPE). A constant phase element can be a consequence of the appearance of a distribution

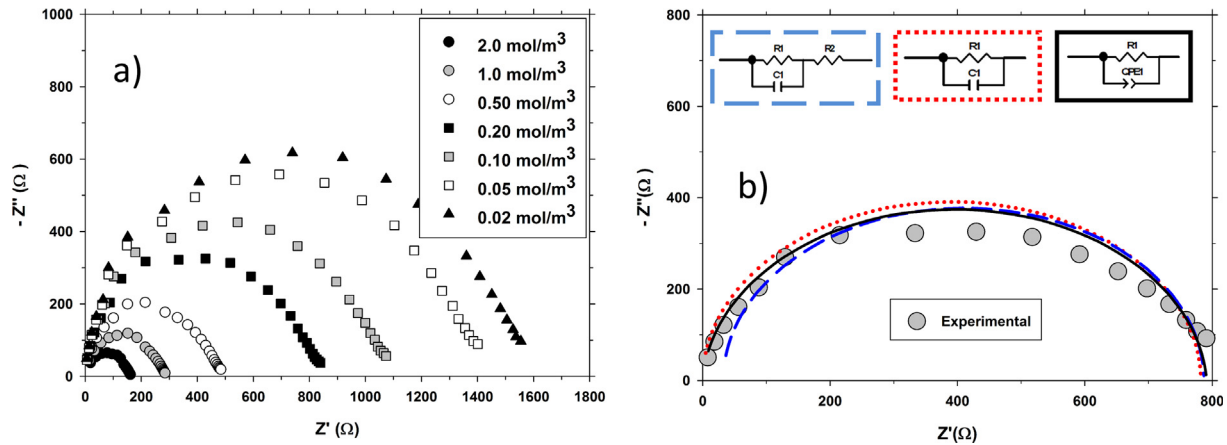


Fig. 9. (a) Z'' versus Z' for the studied KCl concentrations, (b) experimental data on Z'' versus Z' for a 0.20 mol/m³ concentration and fittings for the three equivalent circuits shown in the figure. Note that error bars are not evident because they are below 1% and could not be seen on the plot.

of relaxation times. On electrodes, it has been shown that this phenomenon can be attributed to surface roughness (Levies, 1964, 1965; Scheider, 1975), both from the experimental and theoretical points of view. When analyzing EIS measurements of electrolytes directly on the electrodes, a CPE is generally attributed to a lack of homogeneity on the electrode surface (Brug et al., 1984), because when dealing with liquid electrodes an ideal capacitive behavior is seen (Delahay, 1965) with $n = 1$. Roughness for self-similar surfaces can be characterized by their fractal dimension (Nyikos and Pajkossy, 1985). Therefore, the flattening of the corresponding lobe can be correlated with the surface fractality at the interface membrane-electrodes. According to Pajkossy (Pajkossy, 1991), the fractal dimension D_f is:

$$D_f = \frac{1+n}{n} \quad (22)$$

with n the exponent relating impedance of the CPE with frequency:

$$Z(\omega) = \frac{1}{Q} (j\omega)^{-n} \quad (23)$$

Here ω is the angular frequency and Q is a constant (measured in $F \cdot s^{n-1}$). Fittings as those shown in Fig. 9b give values that correlate well to Eq. (23) with $n = 0.874 \pm 0.006$. If fractal dimension is evaluated by Eq. (22) we get $D_f = 2.144 \pm 0.008$.

Roughness, and fractal dimension (if pores are taken as big depressions on the membrane surface, as even as the responsible for most of roughness), must be the same at the membrane-electrode interface as on the proper membrane surface, when Hg is used as contact liquid. This fractal dimension can be evaluated from AFM results by using the corresponding power spectra density function $\gamma(\vec{\sigma})$ which corresponds to the bi-dimensional roughness spectra and allows to evaluate the fractal dimension as (Carvalho et al., 2011):

$$D_f = \frac{8-n'}{2} \quad (24)$$

where n' is the slope of the function $\gamma(\vec{\sigma})$ in a double logarithmic scale. In our case this procedure leads to $D_f = 2.18 \pm 0.05$. It is apparent that both the values obtained for the fractal dimension fairly agree with each other.

If the most simple circuit is used (dotted lines in Fig. 9b), the capacitance of the condenser C_1 , in parallel with the resistance R_1 , doesn't depend on concentration with a value $C_{pore} = (2.84 \pm 0.16) \cdot 10^{-10}$ F. According to Eq. (14), assuming $\epsilon_{pore} = 80$ leads to a volume porosity of the membrane of $\theta = 0.69 \pm 0.04$. This value is also in a more than fair agreement

with that evaluated in Section 4.1. This proves that, in effect, the dielectric constant inside the pores of our microfiltration membrane doesn't differ from that of bulk water and that pores can be considered as an array of parallel cylinders.

Resistance or conductance values enable us to calculate conductivity by Eq. (12). These values are shown in Fig. 10 and clearly are linearly correlated with the concentration of the solution at both sides of the membrane.

The conductivities in Fig. 10 along with those of the corresponding free solution permit an evaluation of the membrane charge (according to Eq. (20)). In principle both, α and $\kappa_{surface}$, can depend on concentration and, although their correlation is unknown, we can assume, for example, a power function as:

$$\alpha \kappa_{surface} = K(\gamma_{\pm} c)^n \quad (25)$$

That can be substituted in the last term of Eq. (20). Moreover, it is reasonable to assume that the mobilities ratio should be almost concentration independent (Li and Zhao, 2004; Montalvillo et al., 2014). In order to reduce the number of parameters to fit we will use the transport numbers obtained from membrane potential measurements, resulting in a fitted curve as that is shown in Fig. 11. The corresponding parameters are given in Table 3.

The charge of the membrane is quite similar to that obtained from membrane potential measurements (given in Table 2), although now the error range is a little higher. This wide error range is probably mostly due to the assumption of Eq. (25). The

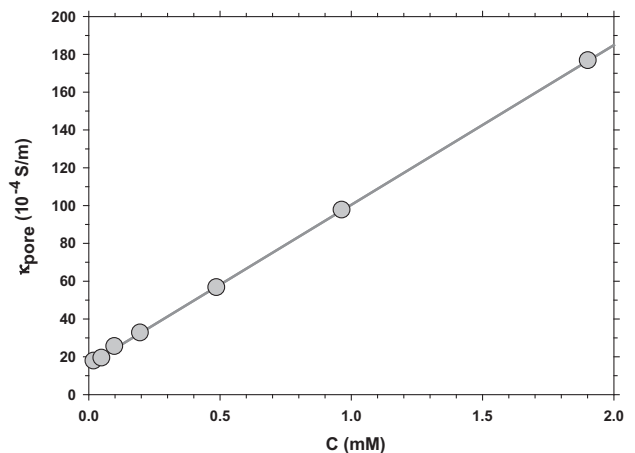


Fig. 10. Conductivity inside pores versus concentration.

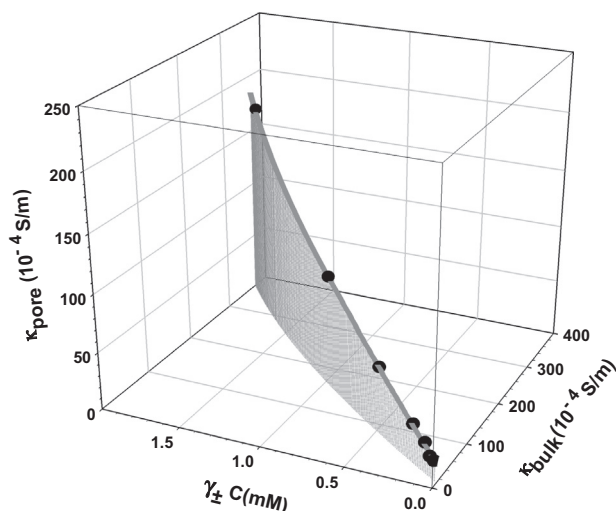


Fig. 11. Fitting of Eq. (20) showing κ_{pore} as a function of κ_{bulk} and $\gamma_{\pm} C$.

Table 3

Parameters obtained from the fitting of Eqs. (20) and (25).

\bar{U}_{-}/U_{-}	0.10 ± 0.08
K	$(5.1 \pm 0.4) \cdot 10^{-3} \Omega^{-1} \text{m}^{(3n-1)} \text{mol}^{-n}$
n	-0.62 ± 0.09
X_m	$19 \pm 4 \text{ mol m}^{-3}$

\bar{U}_{-}/U_{-} ratio is less than unity, again in accordance with the fact that anions have a hindered mobility inside the membrane pores.

Another possibility would be to leave transport numbers as free parameters in Eq. (20) to have now 6 fitting parameters. This procedure would give very big uncertainties to the fitted parameters. Nevertheless, some of the parameters can be grouped to leave 5 free ones strengthening the fitting process. This implies giving up to evaluate, by this procedure, the transport numbers. In such way a membrane charge of $X_m = 22 \pm 1 \text{ mol m}^{-3}$ is obtained. Note that, it is quite similar to that obtained from membrane potential, but with a larger error range. This makes the two characterization methods, both the membrane potential and the impedance spectroscopy, two fully independent techniques to get information on the charge of a microfiltration membrane.

Note that attending to the membrane charge densities, X_m , just evaluated, or that shown in Table 2, and the concentrations range, X_m/C_f ranges from 8 to 1900. Moreover $r_p/\lambda_D \approx 28$. These values guarantee that SC and TMS models would give indistinguishable results (Palmeri et al., 2000; Shang et al., 2006) as already advanced in Section 2.5.

5. Conclusions

In ionic diffusion processes through charged membranes, with small gradients, permeability decreases with the concentration difference. This seems to be correlated with the establishment of ion-membrane charge equilibria on the membrane.

For charged membranes, with pores in the micrometer range, a quite simple model for the membrane potential (with the Donnan equilibria playing the central role) enables us to get the membrane charge density along with the transport numbers inside the pores.

Electrical Impedance Spectroscopy with a mercury containing cell makes simple and easy to assign an equivalent circuit to the ionic transport through the membrane. Of course, this requires an adequate compatibility with the solution and solute to be transported. It has been shown that, in microfiltration membranes with

pores of the micrometric order, the dielectric permittivity inside the pores is equal to the bulk value.

Moreover, it has been shown that the fractality of the membrane surface can accurately explain the observed flattening (in the Nyquist plot) of the lobe corresponding to the ionic transport through the membrane, due to the appearance of a distribution of similar relaxation times. The obtained fractal dimension agrees with that measured by AFM. Therefore, it has been proved that a structural parameter-roughness in this case- in MF membranes can be obtained from Electrical Impedance Spectroscopy.

In addition, EIS has been shown to be able to give the proper charge value of the membrane which agrees within the error range with that obtained from the, more traditional, MP method. This confirms EIS as a valuable, fast and powerful method to get detailed information on the electrical aspects of transport through microfiltration membranes. Of course the equipment needed for EIS is more expensive than that required for MP experiments, but it is faster.

Acknowledgements

Authors thank the Ministerio de Educación y Ciencia (Plan Nacional de I+D+i) through projects CTQ2012-31076 and MAT2016-76413-C2-1-R, Junta de Castilla y León (project VA248U13), PICT 2013-FONCYT and PIP 2014 CONICET Grants. D. R. Díaz acknowledges CPA Fellowship of CONICET to stay at Universidad de Valladolid.

References

- Abràmoff, M.D., Magalhães, P.J., Ram, S.J., 2004. Image processing with image. J. Biophot. Int. 11, 36–42.
- Ariza, M.J., Cañas, A., Benavente, J., 2001. Electrokinetic and electrochemical characterizations of porous membranes. Colloids Surf. A 189, 247–256.
- Barsoukov, E., Macdonald, J.R., 2005. Impedance Spectroscopy. Theory, Experiment, and Applications. John Wiley and Sons, New Jersey.
- Bason, S., Oren, Y., Freger, V., 2007. Characterization of ion transport in thin films using electrochemical impedance spectroscopy: II: examination of the polyamide layer of RO membranes. J. Membr. Sci. 302, 10–19.
- Benavente, J., Fernandez-Pineda, C., 1985. Electrokinetic phenomena in porous membranes: determination of phenomenological coefficients and transport numbers. J. Membr. Sci. 23, 121–136.
- Bowen, W.R., Welfoot, J.S., 2002. Modelling the performance of membrane nanofiltration—critical assessment and model development. Chem. Eng. Sci. 57, 1121–1137.
- Cañas, A., Ariza, M.J., Benavente, J., 2001. Characterization of active and porous sublayers of a composite reverse osmosis membrane by impedance spectroscopy, streaming and membrane potentials, salt diffusion and X-ray photoelectron spectroscopy measurements. J. Membr. Sci. 183, 135–146.
- Carvalho, A.L., Maugeri, F., Silva, V., Hernández, A., Palacio, L., Prádanos, P., 2011. AFM analysis of the surface of nanoporous membranes: application to the nanofiltration of potassium clavulanate. J. Mater. Sci. 46, 3356–3369.
- Cwirko, E.H., Carbonell, R.G., 1992. Ionic equilibria in ion-exchange membranes: a comparison of pore model predictions with experimental results. J. Membr. Sci. 67, 211–226.
- Cheryan, M., 1986. Ultrafiltration Handbook. Technomic Publishing Company, Lancaster, USA.
- Chilcott, T.C., Chan, M., Gaedt, L., Nantawisarakul, T., Fane, A.G., Coster, H.G.L., 2002. Electrical impedance spectroscopy characterisation of conducting membranes. J. Membr. Sci. 195, 153–167.
- Christoforou, C.C., Westermann-Clark, G.B., Anderson, J.L., 1985. The streaming potential and inadequacies of the Helmholtz equation. J. Colloid Interface Sci. 106, 1–11.
- de Lara, R., Benavente, J., 2007. Electrokinetic and surface chemical characterizations of an irradiated microfiltration polysulfone membrane: comparison of two irradiation doses. J. Colloid Interface Sci. 310, 519–528.
- Delahay, P., 1965. The Double Layer and Electrode Kinetics. Interscience, New York.
- Demisch, H.U., Pusch, W., 1979. Electric and electrokinetic transport properties of homogeneous weak ion exchange membranes. J. Colloid Interface Sci. 69, 247–270.
- Efligenir, A., Fievet, P., Déon, S., Salut, R., 2015. Characterization of the isolated active layer of a NF membrane by electrochemical impedance spectroscopy. J. Membr. Sci. 477, 172–182.
- Fievet, P., Szymczyk, A., Labbez, C., Aoubiza, B., Simon, C., Foissy, A., Pagetti, J., 2001. Determining the zeta potential of porous membranes using electrolyte conductivity inside pores. J. Colloid Interface Sci. 235, 383–390.

- Freger, V., Bason, S., 2007. Characterization of ion transport in thin films using electrochemical impedance spectroscopy: I. Principles and theory. *J. Membr. Sci.* 302, 1–9.
- Brug, G.J., van der Eeden, A.L.G., Sluyters-Rehbach, M., Sluyters, J.H., 1984. The analysis of electrode impedances complicated by the presence of a constant phase element. *J. Electroanal. Chem.* 176, 275–295.
- Galama, A.H., Post, J.W., Hamelers, H.V.M., Nikonenko, V.V., Biesheuvel, P.M., 2016. On the origin of the membrane potential arising across densely charged ion exchange membranes: how well does the Teorell-Meyer-Sievers theory work? *J. Membr. Sci. Res.* 2, 128–140.
- Hernández, A., Calvo, J.I., Prádanos, P., Tejerina, F., 1996. Pore size distributions in microporous membranes. A critical analysis of the bubble point extended method. *J. Membr. Sci.* 112, 1–12.
- Hernández, A., Ibáñez, J.A., Martínez-Villa, F., Arribas, J.I., Martín-salas, A., Tejerina, A.F., 1986. On the effect of the porosities of microporous membranes on their ionic selectivities. *J. Membr. Sci.* 27, 131–141.
- Hernandez, A., Martinez, F., Martín, A., Prádanos, P., 1995. Porous structure and surface charge density on the walls of microporous alumina membranes. *J. Colloid Interface Sci.* 173, 284–296.
- Honda, M., 2009. *Agilent Impedance Measurement Handbook. A guide to Measurement Technology and Techniques*. Agilent Technologies ed., USA.
- Jacob, J., Prádanos, P., Calvo, J.I., Hernández, A., Jonsson, G., 1998. Fouling kinetics and associated dynamics of structural modifications. *Colloids Surf. A* 138, 173–183.
- Kontturi, K., Mafé, S., Manzanares, J.A., Pellicer, J., Vuoristo, M., 1994. A new method for determining transport numbers of charged membranes from convective diffusion experiments. *J. Electroanal. Chem.* 378, 111–116.
- Nyikos, L., Pajkossy, T., 1985. Fractal dimension and fractional power frequency-dependent impedance of blocking electrodes. *Electrochim. Acta* 30, 1533–1540.
- Lakshminarayanaiah, N., 1965. Transport phenomena in artificial membranes. *Chem. Rev.* 65, 491–565.
- Lakshminarayanaiah, N., 1969. *Transport Phenomena in Membranes*. Academic Press, New York.
- Lakshminarayanaiah, N., 1975. Measurement of membrane potential and estimation of effective fixed-charge density in membranes. *J. Membr. Biol.* 21, 175–189.
- Lakshminarayanaiah, N., 1984. *Equations of Membrane Biophysics*. Academic Press, Inc., New York.
- Levies, R.D., 1964. On porous electrodes in electrolytesolutions-IV. *Electrochim. Acta* 9, 1231–1245.
- Levies, R.D., 1965. The influence of surface roughness of solid electrodes on electrochemical measurements. *Electrochim. Acta* 10, 113–130.
- Li, Y.H., Zhao, K.S., 2004. Dielectric analysis of nanofiltration membrane in electrolyte solutions: influences of electrolyte concentration and species on membrane permeation. *J. Colloid Interface Sci.* 276, 68–76.
- Lonsdale, H.K., Merten, U., Riley, R.L., 1965. Transport properties of cellulose acetate osmotic membranes. *J. Appl. Polym. Sci.* 9, 1341–1362.
- Lyklema, J., Minor, M., 1998. On surface conduction and its role in electrokinetics. *Colloids Surf. A* 140, 33–41.
- Macdonald, J.R., 1987. *Impedance Spectroscopy. Emphatizing Solid Materials and Systems*. John Wiley and Sons, New York.
- Mafe, S., Manzanares, J.A., Ramirez, P., 2003. Modeling of surface vs. bulk ionic conductivity in fixed charge membranes. *PCCP* 5, 376–383.
- Martínez-Villa, F., Martínez, L., Arribas, J.I., Tejerina, F., 1988. Effects of structure and charge on the diffusive salt permeation across microporous membrane filters. *J. Membr. Sci.* 36, 31–44.
- Martínez, F., Martín, A., Malfaito, J., Palacio, L., Prádanos, P., Tejerina, F., Hernández, A., 2002. Streaming potential through and on ultrafiltration membranes: Influence of salt retention. *J. Membr. Sci.* 206, 431–441.
- Mikhaylin, S., Bazinet, L., 2016. Fouling on ion-exchange membranes: classification, characterization and strategies of prevention and control. *Adv. Colloid Interface Sci.* 229, 34–56.
- Montalvillo, M., Silva, V., Palacio, L., Calvo, J.I., Carmona, F.J., Hernández, A., Prádanos, P., 2014. Charge and dielectric characterization of nanofiltration membranes by impedance spectroscopy. *J. Membr. Sci.* 454, 163–173.
- Nagasawa, M., Kobatake, Y., 1952. The theory of membrane potential. *J. Phys. Chem.* 56, 1017–1024.
- Pajkossy, T., 1991. Electrochemistry at fractal surfaces. *J. Electroanal. Chem. Interfacial Electrochem.* 300, 1–11.
- Palmeri, J., Blanc, P., Larbot, A., David, P., 1999. Theory of pressure-driven transport of neutral solutes and ions in porous ceramic nanofiltration membranes. *J. Membr. Sci.* 160, 141–170.
- Palmeri, J., Blanc, P., Larbot, A., David, P., 2000. Hafnia ceramic nanofiltration membranes. *J. Membr. Sci.* 179, 243–266.
- Pinelo, M., Møller, V., Prado-Rubio, O.A., Jonsson, G., Meyer, A.S., 2013. Mechanisms controlling retention during ultrafiltration of charged saccharides: molecular conformation and electrostatic forces. *Sep. Purif. Technol.* 118, 704–709.
- Robinson, R.A., Stokes, R.H., 2002. *Electrolyte Solutions*. Dover, London.
- Romero, V., Vázquez, M.I., Benavente, J., 2013. Study of ionic and diffusive transport through a regenerated cellulose nanoporous membrane. *J. Membr. Sci.* 433, 152–159.
- Schaep, J., Vandecasteele, C., Leysen, R., Doyen, W., 1998. Salt retention of Zirfon® membranes. *Sep. Purif. Technol.* 14, 127–131.
- Scheider, W., 1975. Theory of the frequency dispersion of electrode polarization. Topology of networks with fractional power frequency dependence. *J. Phys. Chem.* 79, 127–136.
- Shang, W.-J., Wang, X.-L., Yu, Y.-X., 2006. Theoretical calculation on the membrane potential of charged porous membranes in 1-1, 1-2, 2-1 and 2-2 electrolyte solutions. *J. Membr. Sci.* 285, 362–375.
- Siddiqi, F.A., Prakash, P., Singh, S.P., 1978. Studies with model membranes. *Colloid Polym. Sci.* 256, 552–562.
- Silva, V., Martín, Á., Martínez, F., Malfaito, J., Prádanos, P., Palacio, L., Hernández, A., 2011. Electrical characterization of NF membranes. A modified model with charge variation along the pores. *Chem. Eng. Sci.* 66, 2898–2911.
- Silva, V., Montalvillo, M., Carmona, F.J., Palacio, L., Hernández, A., Prádanos, P., 2016. Prediction of single salt rejection in nanofiltration membranes by independent measurements. *Desalination* 382, 1–12.
- Starzak, M.E., 1984. *The Physical Chemistry of Membranes*. Academic Press, New York.
- Takagi, R., Nakagaki, M., 1996. Membrane charge of microporous glass membrane determined by the membrane potential method and its pore size dependency. *J. Membr. Sci.* 111, 19–26.
- Tanaka, Y., 2015. *Ion Exchange Membranes, Fundamentals and Applications*. Elsevier, Amsterdam.
- Tanninen, J., Mänttari, M., Nyström, M., 2007. Effect of electrolyte strength on acid separation with NF membranes. *J. Membr. Sci.* 294, 207–212.
- Westermann-Clark, G.B., Anderson, J.L., 1983. Experimental verification of the space-charge model for electrokinetics in charged microporous membranes. *J. Electrochem. Soc.* 130, 839–847.
- Xu, T., 2005. Ion exchange membranes: atate of their development and perspective. *J. Membr. Sci.* 263, 1–29.
- Yang, J., Bellmann, C., Grundke, K., Michel, S., Kostiuk, L., Kwok, D.Y., 2003. Characterization of porous membranes by zeta-potential under an ac electric field: analytical treatment of time-dependent electroosmotic flow. *J. Membr. Sci.* 225, 155–164.
- Yaroshchuk, A.E., 2001. Non-steric mechanisms of nanofiltration: superposition of Donnan and dielectric exclusion. *Sep. Purif. Technol.* 22–23, 143–158.
- Zhao, K., Ni, G., 2011. Dielectric analysis of nanofiltration membrane in electrolyte solutions: influences of permittivity of wet membrane and volume charge density on ion permeability. *J. Electroanal. Chem.* 661, 226–238.
- Zhao, K., Yasuhiro, M., Asaka, K., Asami, K., Hanai, T., 1991. Dielectric analysis of concentration polarization phenomena at cation-exchange membrane/solution interfaces by frequency variation and d.c. bias application. *J. Membr. Sci.* 64, 163–172.